The influence of acceleration loading curve characteristics on traumatic brain injury

Andrew Post[a], T. Blaine Hoshizaki[a], Michael D. Gilchrist[b,a], Susan Brien[c,a], Michael Cusimano[d], and Shawn Marshall[e]

Human Kinetics, University of Ottawa, Ottawa, Canada[a]

School of Mechanical & Materials Engineering, University College Dublin, Dublin, Ireland[b]

Hull Hospital, Gatineau, Canada[c]

St. Michael's Hospital, Toronto, Canada[d]

Ottawa General Hospital, Ottawa, Canada[e]

Corresponding author: Andrew Post (apost@uottawa.ca) 200 Lees Ave., room A106, Ottawa, Ontario, Canada, K1N 6N5 – phone number: +1 (613)5625800 ext 7210

Word count: 3,082

Abstract

To prevent brain trauma understanding the mechanism of injury is essential. Once the mechanism of brain injury has been identified, prevention technologies could then be developed to aid in their prevention. The incidence of brain injury is linked to how the kinematics of a brain injury event affects the internal structures of the brain. As a result it is essential that an attempt be made to describe how the characteristics of the linear and rotational acceleration influence specific traumatic brain injury lesions. As a result, the purpose of this study was to examine the influence of the characteristics of linear and rotational acceleration pulses and how they account for the variance in predicting the outcome of TBI lesions, namely contusion, subdural hematoma (SDH), subarachnoid hemorrhage (SAH), and epidural hematoma (EDH) using a principal components analysis (PCA). Monorail impacts were conducted which simulated falls which caused the TBI lesions. From these reconstructions, the characteristics of the linear and rotational acceleration were determined and used for a PCA analysis. The results indicated that peak resultant acceleration variables did not account for any of the variance in predicting TBI lesions. The majority of the variance was accounted for by duration of the resultant and component linear and rotational acceleration. In addition, the components of linear and rotational acceleration characteristics in x, y, and z accounted for the majority of the remainder of the variance after duration.

Keywords: Traumatic brain injury, principle components analysis, kinematics

Introduction

Understanding the mechanism of injury for brain trauma is very important in developing prevention technologies and avoidance strategies to prevent impacts associated with those injuries. The inability to obtain direct measures on human subjects to study the underlying mechanics of injury has led to employing animal, physical and numerical models (Ommaya et al., 1971; Zhang et al., 2004). Several researchers have published review articles summarizing brain injury mechanism research using these methods (King et al., 2003; Hardy et al., 1994; Viano et al., 1989). This research describes the mechanism of brain injury as linked to damaging levels of brain tissue deformation caused by linear and rotational acceleration (Viano et al., 1989; Kleiven, 2007).

The characteristics of linear and rotational acceleration loading affect tissue compression, tension and shearing which can be measured using computational models of the human brain (Gurdjian and Webster, 1947; Kleiven, 2007; Post and Hoshizaki, 2012). The response of tissue to anatomical testing methods also suggests that the brain is sensitive to rates and direction of loading (Darvish et al., 2001; Hrapko et al., 2006). Strain dependent nature of brain tissue has also been reported by Nicolle et al. (2004). In addition, other researchers have observed that during high speed impacts neural tissue behaves differently at high frequency when compared to low frequency (Rashid et al, 2012a/b). The method of loading of the brain tissue for tolerance testing has also been documented to produce varying failure rates (Lee and Hault, 1989; Monson et al., 2003) and Arbogast and Margulies (1997) as well as Donnelly and Medige (1997) demonstrated that brain material response was dependent on loading rate and particularly in the brainstem.

The mechanical response of the brain is linked to the kinematics of the event, which are typically measured using linear and angular acceleration loading curves (Post and Hoshizaki, 2012). As a result, how the tissue in the brain is loaded, where it is loaded, and the magnitude of that loading is dependent on these kinematic variables. How this loading affects brain tissue is determined by the characteristics of the tissue itself. Researchers have investigated the influence of loading curve shape and direction on tissue deformation metrics associated with brain injury (Willinger and Baumgartner, 2003; Zhang et al., 2004; Kleiven 2007). Kleiven (2006) used a finite element model to evaluate the influence of kinematic dependent variables on intracranial strains causing mTBI. Using pure rotational and translational pulses of sinusoidal shape with magnitudes reflecting severities thought to be associated with concussion, Kleiven found that pure rotational pulses showed the best correlation with strain in the FE model. When comparing the translational pulses to strain, the head impact criterion and head impact power showed the best correlation (Kleiven 2006). Kleiven did not however discuss the influence of the curve characteristics on the intracranial strains, but simply identified the level of correlation between peak values. In an attempt to examine the influence of time to peak on maximum principal strain and Von Mises stress, Post et al. (2012a) produced artificial acceleration loading curves and found that dissimilar shaped curves with identical peak values and area produced different magnitudes of brain deformation. These results suggest that peak resultant values are not the sole contributor to injurious brain deformation. They concluded from this research that while it is evident that various characteristics of the acceleration loading curve, such as slope to peak and total duration, are influential in the production of brain deformation, an examination of linear and angular acceleration causing a brain injury was necessary as the next step. The same authors attempted a more refined analysis of hockey helmet impacts to examine how the kinematic

variables influenced the magnitude of stress and strain within a finite element model of the human brain (Post et al., 2012b). They found that rotational acceleration loading curve characteristics had a stronger relationship with maximum principal strain and von Mises stress than linear acceleration (Post et al., 2012b). The authors of these studies did not, however, have reconstructions of actual injuries with which to examine the influence of the kinematic variables, and were thus limited to discussing possible trends between linear and rotational acceleration and brain deformation metrics.

The purpose of this study was to examine the influence of the characteristics of linear and rotational acceleration and how they account for the variance in predicting the outcome of TBI lesions incurred from falls using a principal components analysis. The TBI lesions that were analyzed were: contusion, subdural hematoma (SDH), subarachnoid hemorrhage (SAH), and epidural hematoma (EDH).

Methods

Head injury reconstructions

Twenty adult subjects who incurred a TBI lesion from simple falls were recruited for this research (Tables 1, 2, and 3). Each subject signed informed consent and all procedures concerning the contact and use of data followed approved ethical guidelines. The subjects were recruited from the Hull Hospital (Gatineau, Quebec, Canada), Ottawa General Hospital (Ottawa, Ontario, Canada), and the National Department of Neurosurgery at Beaumont Hospital, Dublin, Ireland. For the subjects to be recruited they had to have incurred a TBI lesion from a simple fall, where there was no contact with another person or object before or during the fall. In addition, each subject had no previous head injury or neurological defect. For each case, CT and/or MRI

scans were conducted within 24 hours of incurring the injury from the falling event. Each CT/MRI scan was analyzed for the presence of a TBI lesion by the radiologist and neurosurgeon at the hospital. In many cases the medical imaging was confirmed by surgical interventions. For the purpose of the laboratory reconstruction, injury report forms filled out by the patient and/or eyewitnesses as well as video (if available) of the event were used to ascertain the initial conditions of each fall simulation. The form gave information such as: establishing likely starting body position, impact surface, and location of impact on the head (which was also confirmed by CT scan in many cases by the presence of a scalp contusion). The process of reconstructing the falling event was conducted in two parts. First, a MAthematical DYnamic MOdels (MADYMO) simulation was run of the incident to establish the possible inbound velocities of the head when it made contact with the surface accounting for the most likely body positions. Second, a Hybrid III headform and neckform attached to a monorail device was used to simulate the impact, with the surface defined by the report form and velocity by the MADYMO reconstruction. In many cases the impact surface was concrete and steel, which is a highly non-compliant material, while there were also wood, and carpet impacts. Of these impact surfaces the carpet reconstruction had the most variance, but in fact this variance was very small (less than 1% in linear and rotational acceleration).

MADYMO reconstructions

Mathematical dynamic models is a tool which has been commonly used to reconstruct the kinematics of the human body for falling scenarios. This software has a particular strength in that it has a variety of ellipsoid pedestrian models which have joint parameters similar to those of a human (O'Riordain et al., 2003). This tool allows for the simulation of the events leading up to the head contact to the ground (in this case) which makes it possible to approximate the head

impact velocity while taking into account the motions of the body as the fall takes place. The ellipsoid pedestrian models used in this research were validated using various impactors that were designed to determine the risk to pedestrians from vehicle impacts.

For each fall reconstruction, a series of MADYMO simulations were conducted using an ellipsoid pedestrian model which was closest to the anthropometry of the human subject. The model was placed within the accident environment in a similar position to the starting position as described in the accident reports forms and eyewitness reports (Adamec et al., 2010). As report forms inherently have some variability in their accuracy concerning the actual event, a sensitivity analysis of each case was run with a series of possible impact scenarios conducted (Figure 1) (O'Riordain et al., 2003; Forero Rueda and Gilchrist, 2009; Adamec et al., 2010). For each injury reconstruction, a minimum of three MADYMO simulations were conducted to ensure that the contact head velocity at impact was properly framed with a slowest possible and fastest possible value. These velocities were then used as the target velocities for the Hybrid III headform drops using a monorail drop rig (Table 1).

Equipment

The physical reconstructions used the monorail drop rig outfitted with a Hybrid III headform and neckform (Figure 2). The monorail was 4.7 m high and had a drop carriage to which the Hybrid III 50% headform and neckform was affixed. Upon release, the headform dropped vertically on ball bushings until contact with the impacting surface. The release mechanism was a pneumatic piston to ensure a clean drop, and the contact velocity was determined by photoelectric time gate within 2.6 cm of impact. The impact location on the headform was determined by the accident reports and CT/MRI scans (Figure 3). The impact surfaces were determined from the injury report forms and are described in table 1 for each case.

For each velocity three impacts were conducted per subject and all were included in the principal components analysis. The variation of the resulting linear and rotational accelerations was low between the three impacts for all reconstructions.

The Hybrid III 50% headform was outfitted with a 3-2-2-2 accelerometer array (Padgaonkar et al., 1975) and sampled at 20 kHz. The accelerometers used were Endevco 7264C-2KTZ-2-300. The resulting signal was filtered using a 1650 Hz low pass butterworth filter. All signals were collected using a DTS prolab module and stored on a computer. The x-axis was defined as facing forward from the head centre of gravity, the y-axis to the left of the head and the z-axis vertically upwards.

Curve characteristic analysis

The linear and angular acceleration curve characteristics producing the specific lesion type (contusion, subdural hematoma, subarachnoid hemorrhage, epidural hematoma) was evaluated using a principal component analysis (PCA) approach. The influence of peak value, total duration and time to peak (Figure 4) on outcome TBI lesion was conducted. The integral of the linear and angular acceleration time curve for the resultant and all components was also calculated. In addition average slope to peak (defined as peak magnitude over time) was calculated to examine if a combination of peak magnitude and the time to that magnitude had any influence on the resulting lesion.

Results

Contusion

There were 6 cases of contusion in the dataset. The principal components analysis with varimax (orthogonal rotation) disclosed a 4 component solution, which accounted for 93 % of the

variance (table 4). Component 1 consisted of the time to peak components of the characteristics of linear and angular acceleration leading to contusion lesions, which accounted for 37 % of the total variance. Component 2, which accounted for 23.8 % of the total variance, consisted of the peak, slope and integrals of the x linear and y angular components. The third component comprised of y axis linear peak, slope and integral accounted for an additional 21.1 % of the total variance. Finally, component 4 represented z axis peak, slope and integral in linear acceleration, which accounted for 11.1 % of the total variance.

Subdural hematoma

There were 16 cases of subdural hematoma in the dataset. For subdural hematoma, the PCA identified a 4 component solution which accounted for 85.1 % of the total variance (table 5). Component one consisted of time to peak variables and total duration which accounted for 36.3 % of the total variance. Component 2 comprised of x angular loading curve peak magnitude, slope, and integral, which accounted for 18.7 % of the total variance. The third component consisted of x axis linear acceleration peak, slope, and integral, as well as y axis peak and integral, accounting for 18.2 % of the total variance. Finally, component 4 consisted of z axis peak, slope, and integral, accounting for a further 12 % of the total variance.

Subarachnoid hemorrhage

There were 5 cases of subarachnoid hemorrhage in the dataset. For subarachnoid hemorrhage, the PCA also identified a 4 component solution, which accounted for 93.1 % of the total variance (table 6). The first component consisted of the time to peak variables for the resultant, x, and y axis as well as the total duration of the pulse, which accounted for 36.3 % of the total variance.

The second component consisted of x axis linear, and y axis angular loading curve peak, slope, and integral values, accounting for 23.9 % of the total variance. The third component consisted of x angular peak and slope as well as and z axis peak, slope, and integral, which accounted for 21.8 % of the variance. Finally, the fourth component consisted of z axis linear peak and slope, accounting for 11.1 % of the variance.

Epidural hematoma

There were two cases of epidural hematoma in the dataset. For the epidural hematoma, the PCA identified a 2 component solution, which accounted for 94.6 % of the total variance (table 7). The first component consisted of the resultant linear and angular time to peak values, as well as x and y linear and angular time to peak. The first component also consisted of y axis angular acceleration peak, and z angular acceleration slope values, as well as total duration of the pulse. Overall, the first component accounted for 57.4 % of the total variance. The second component consisted of the x and y axis linear acceleration peak, slope, and integral, as well as the z axis angular integral, accounting for a further 37.2 % of the total variance.

Discussion

Contusion

The results of the PCA identified time to peak resultant and component in x and y characteristics of the linear and angular acceleration the best predictors for contusions. The total duration of the pulse was also important. The influence of the z axis on the variance was low, probably as a result of there being no top of the head impacts in this dataset. When examining the components, only the x angular characteristics and the y linear and angular characteristics accounted for part

of the variance and not the resultant characteristics such as peak, slope or integral. These results indicate that resultant loading curve characteristics, other than linear and angular time to peak, had little influence on the variance of the dataset producing a contusion.

Subdural hematoma

Like the contusion result, the PCA identified time based variables such as time to peak for the linear and angular acceleration in x and y component as well as resultant accounted for a large part of the variance. Total duration was also found to be influential. Interestingly, the results show more variance was accounted for by the angular components in x, y, and z axes (30 % +) than the x axis linear curve characteristics. These results would suggest that the angular acceleration characteristics accounted for more variance than the linear acceleration characteristics. The lack of resultant loading curve characteristics accounting for very much of the total variance is likely a result of the components being more closely associated with the event. This is in agreement with previous literature which has identified subdural hematoma as a rotationally influenced lesion as opposed to a linear dominant injury similar to other forms of TBI (Kleiven, 2003).

Subarachnoid hemorrhage

As with contusion and subdural hematoma, the PCA for subarachnoid hemorrhage indicated a large amount of the variance to be accounted for by time to peak and total duration characteristics. The remaining components involve x and z linear curve characteristics and x, y, and z angular curve characteristics. Like subdural hematoma, a large amount of the variance, after the time based characteristics, is accounted for by angular loading curve peak, slope, and

integral. This indicates a rotational influence for the risk of subarachnoid hemorrhage which is based within the x, y, and z components and not the characteristics of the resultant linear or angular acceleration.

Epidural hematoma

There was a low sample size of reconstructions which produced an epidural hematoma (2). As a result the PCA extracted 2 components which accounted for 94.6 % of the total variance. The first component was time based, which was similar to the other TBI lesions. The second component was mostly x and y axis linear dynamic response characteristics. Overall, after the linear and angular time to peak values in x, y, and z axes, the characteristics of the linear acceleration loading curve appeared to account for more variance in the cases involving epidural hematoma.

Conclusion

In conclusion, the PCA showed that both linear and angular acceleration accounted for variance in the dynamic response which incurred contusion, SDH, SAH, or EDH. Of particular interest was that the resultant curve characteristics of slope, integral, or peak did not appear to account for any of the variance. This result suggests that using components of the linear and angular acceleration loading curve in x, y, and z axes may account for more variance in the production of these TBI than the resultant values alone. This reinforces the usefulness of tools such as finite element modeling of the human brain to measure brain deformation responses using the

components of linear and angular acceleration as this method can quantify the influence these curve characteristics have on the outcome.

The fact that the results show that time of the pulse and time to peak variables have importance when it comes to TBI, reinforces the use of integrations such as Gadd severity index (GSI) and the Head impact criterion (HIC) as they attempt to use duration to influence the predictions of injury risk (Gadd, 1966; Versace, 1971). However, the GSI and HIC are not particularly predictive of injury (Goldsmith, 1981), which may be in part due to time based considerations only accounting for around 38 % of the variance of TBI as well as no rotational components. The reconstructions in this study led to extremely short duration time to peak (0.0017 s) and duration (0.03) linear and angular accelerations. The intervention of protective devices (helmets, crash pads etc) serve to lengthen this response, but may as a result create longer pulses which have been associated with the occurrence of mTBI (Wright et al., 2012). As a result it would be interesting for future research to investigate mTBI dynamic response and examine curve characteristics which may differentiate between TBI and mTBI.

Limitations

Limitations of this study revolve around the accuracy of the reconstruction and the modeling process from the previous work simulating brain injuries. The reconstructions conducted within the laboratory use non biofidelic physical models which produce linear and angular accelerations which may not be similar to the response of a non-rigid system such as the human head. The input parameters (velocity, mass, location) are all calculated and may not accurately represent the event, while using multiple conditions for each injury simulation may cover the actual event; it is unlikely a precise representation of the event causing the injury will

be simulated. The influence of the musculature on the impact will also be difficult to ascertain and is thus also a limitation to this study. While simple to reconstruct injury scenarios were chosen for this study, it is unlikely that each simulation was exact to the individual who was injured. The variables chosen to reflect the characteristics of the acceleration loading curve do not reflect all possible combinations of time and peak variable. As such it is possible that a curve characteristic not analyzed here could account for a larger amount of the variance.

Acknowledgements

Funding was provided for this research by the Canadian Institutes of Health Research

Conflict of interest statement

There are no conflicts of interest with the submitted research.

References

1. Arbogast, K.B., Margulies, S.S., 1998. Material characterization of the brainstem from oscillatory shear tests. Journal of biomechanics 31(9), 801-807.

2. Darvish, K.K., Crandall, J.R., 2001. Nonlinear viscoelastic effects in oscillatory shear deformation of brain tissue. Medical Engineering and Physics 23(9), 633-645.

3. Donnelly, B.R., Medige, J., 1997. Shear properties of human brain tissue. Journal of Biomechanical Engineering 119(4), 423-432.

4. Gadd, C.W., 1966. Use of a weighted impulse criterion for estimating injury hazard. In Proceedings of the 10th Stapp Car Crash Conference, SAE paper No. 660793.

5. Goldsmith, W., 1981. Current controversies in the stipulation of head injury criteria. Letter to the editor. Journal of Biomechanics 14, 883-884.

6. Gurdjian, E.S., Webster, J.E., 1947. The mechanism and management of injuries to the head. Journal of the American Medical Association 134(13), 1072-1077.

7. Hardy, W.N., Khalil, T.B., King, A.I., 1994. Literature review of head injury biomechanics. International Journal of Impact Engineering 15(4), 561-568.

8. Hrapko, M., van Dommelen, J.A.W., Peters, G.W.M., Wismans, J.S., 2006. The mechanical behaviour of brain tissue: Large strain response and constitutive modeling. Biorheology 43(5), 623-636.

9. King, A.I., Yang, K.H., Zhang, L., Hardy, W., Viano, D.C., 2003. Is head injury caused by linear or angular acceleration. In Proceedings of the IRCOBI Conference, Lisbon, Portugal.

10. Kleiven, S., 2006. Evaluation of head injury criteria using a finite element model validated against experiments on localized brain motion, intracerebral acceleration, and intracranial pressure. International Journal of Crashworthiness 11 (1), 65-79.

11. Kleiven, S., 2007. Predictors for traumatic brain injuries evaluated through accident reconstruction. Stapp Car Crash Journal 51, 81-114.

12. Lee, M.C., Hault, R.C., 1989. Insensitivity of tensile failure properties of human bridging veins to strain rate: implications in biomechanics of subdural hematoma. Journal of Biomechanics 22(6-7), 537-542.

13. Monson, K.L., Goldsmith, W., Barbaro, N.M., Manle, G.T., 2003. Axial mechanical properties of fresh human cerebral blood vessels. Journal of Biomedical Engineering 125(2), 288-294.

14. Nicolle, S., Lounis, M., Willinger, R., 2004. Shear properties of brain tissue over a frequency range relevant for automotive impact situations: New experimental results. Stapp Car Crash Journal 48, 239-258.

15. Ommaya, A.K., Grubb, R.L., Naumann, R.A., 1971. Coup and contrecoup injury: Observations in the mechanics of visible brain injuries in the rhesus monkey. Journal of Neurosurgery 35- 503-516.

16. Padgaonkar, A.J., Kreiger, K.W., King, A.I., 1975. Measurement of angular acceleration of a rigid body using linear accelerometers. Journal of Applied Mechanics 42, 552-556.

17. Post, A., Hoshizaki, T.B., 2012. Mechanical properties describing brain impact injuries: A review. Trauma 14(4), 327-349.

18. Post, A., Hoshizaki, T.B., Gilchrist, M.D., 2012a. Finite element analysis of the effect of loading curve shape on brain injury predictors. Journal of Biomechanics 45, 679-683.

19. Post, A., Walsh, E.S., Hoshizaki, T.B., Gilchrist, M.D., 2012b. Analysis of loading curve characteristics on the production of brain deformation metrics. Journal of Sports Engineering and Technology 226(3/4), 200-207.

20. Rashid, B., Destrade, M., Gilchrist, M.D., 2012a. Mechanical characterization of brain tissue in compression at dynamic strain rates. Journal of the Mechanical Behavior of Biomedical Materials 10, 23-38.

21. Rashid, B., Destrade, M., Gilchrist, M.D., 2012b. Mechanical characterization of brain tissue in tension at dynamic strain rates. Journal of the Mechanical Behavior of Biomedical Materials, in press.

22. Versace, J., 1971. A review of the severity index. In Proceedings of the 15th STAPP Car Crash Conference, SAE paper No. 710881.

23. Viano, D.C., King, A.I., Melvin, J.W., Weber, K., 1989. Injury biomechanics research: An essential element in the prevention of trauma. Journal of Biomechanics 22(5), 403-417.

24. Willinger, R., Baumgartner, D., 2003. Numerical and physical modelling of the human head under impact – towards new injury criteria. International Journal of Vehicle Design 32, 94-115.

25. Wright, R., Post, A., Hoshizaki, T.B., Ramesh, K.T., 2012. A computational approach to estimate axonal damage under inertial loading of the head. Journal of Neurotrauma, in press

26. Zhang, L., Yang, K.H., King, A.I., 2004. A proposed injury threshold for mild traumatic brain injury. Journal of Biomechanical Engineering 126, 226-236.

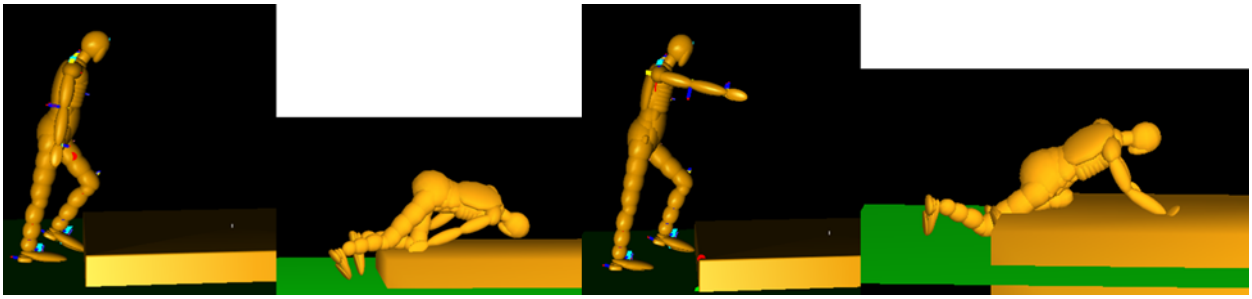

Figure 1. Two MADYMO reconstructions of two extremes for a falling simulation: (left) trip with no arms to brace the fall; and (right) arms held out to brace against the fall

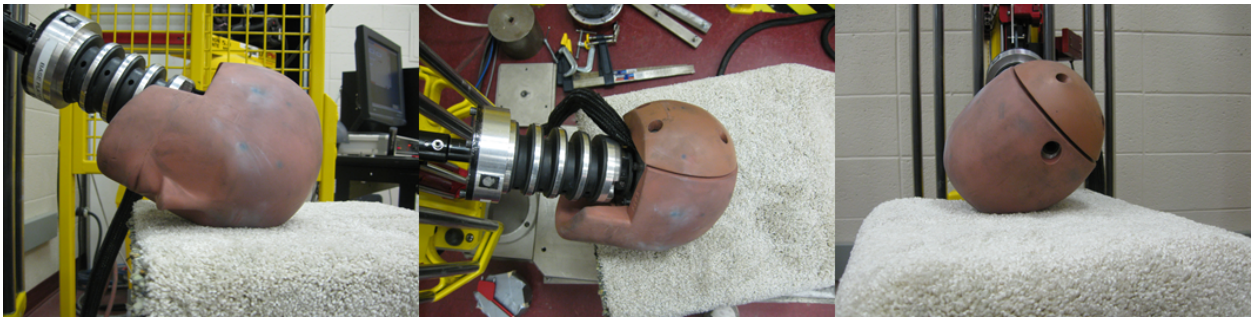

Figure 2. Physical reconstruction using a Hybrid III headform and neckform for a fall onto a carpet with underlay covering a concrete anvil

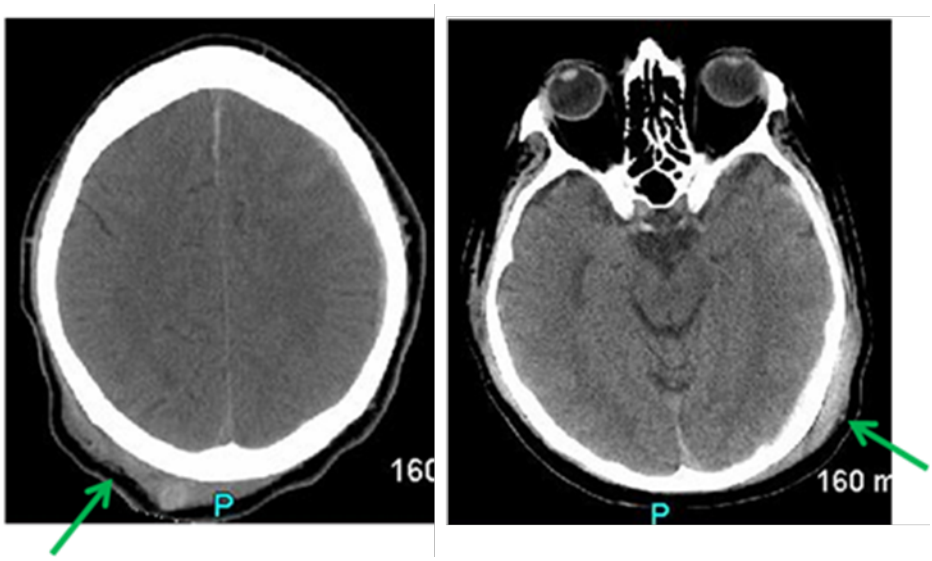

Figure 3. CT scans showing the impact location on the skull as shown by extradural hematoma (designated by arrows)

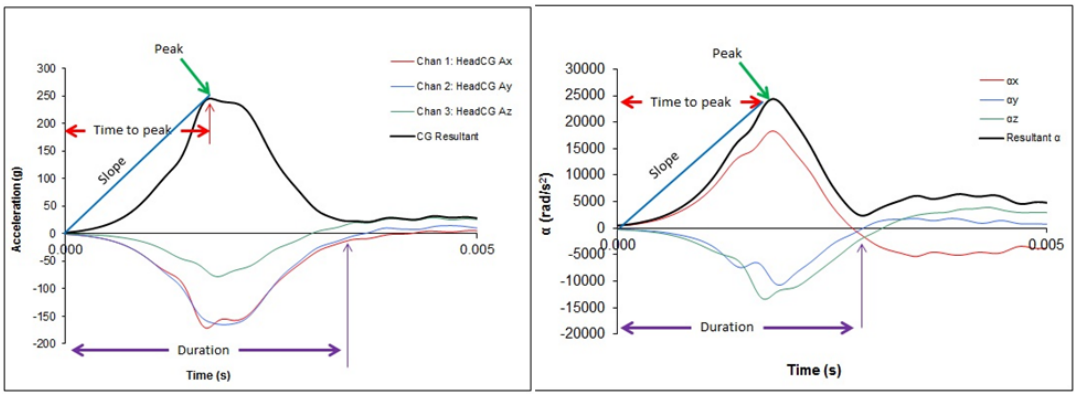

Figure 4. Linear (right) and angular (left) acceleration loading curve characteristic breakdown using resultant acceleration curves as an example.

Table 1. Impact velocities and surfaces of the reconstructions

Case #	Velocity (m/s)	Surface	TBI Lesion
1	3.0 - 4.0	Concrete	Subdural Hematoma
2	4.7 - 5.2	Concrete	Subdural Hematoma
3	5.1 - 6.1	Concrete	Subdural Hematoma; Epidural Hematoma; Contusion
4	4.1 - 5.4	Concrete	Subarachnoid Hemorrhage
5	3.9 - 6.2	Wood	Subdural Hematoma; Subarachnoid Hemorrhage
6	2.2 - 3.3	Carpet	Subdural Hematoma
7	3.9 - 6.2	Concrete	Subdural Hematoma; Subarachnoid Hemorrhage; Contusion
8	3.3 - 4.8	Concrete	Subdural Hematoma
9	4.8 - 6.2	Concrete	Subdural Hematoma; Subarachnoid Hemorrhage;
10	3.6 - 4.9	Concrete	Subarachnoid Hemorrhage; Contusion
11	3.7 - 5.8	Concrete	Subdural Hematoma; Contusion
12	3.6 - 4.8	Concrete	Epidural Hematoma
13	4.8 - 6.2	Wood	Subdural Hematoma
14	3.8 - 6.0	Concrete	Subdural Hematoma; Contusion
15	4.8 - 5.8	Concrete	Parenchymal Hemorrhage; Contusion
16	5.1 - 5.6	Concrete	Subdural Hematoma
17	4.5 - 4.8	Concrete	Subdural Hematoma
18	3.5 - 4.2	Concrete	Subdural Hematoma
19	4.7 - 5.1	Concrete	Subdural Hematoma
20	5.4 - 6.1	Metal bar	Subdural Hematoma

Table 2. Impact locations and lesion types of reconstructions 1-10. Fr = frontal; Temp = temporal; Par = Parietal; Occ = Occipital.

Case #	Impact location	Location of lesion	TBI Lesion
1		Right Frontal	SDH
2		Right Frontal	SDH
3	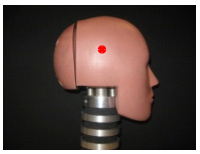	Frontal/Occipital	SDH/Contusion (Fr); EDH (Occ)
4	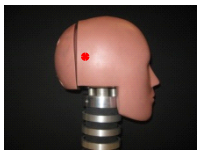	Frontal/Parietal	Contusion (Fr); SAH (Par)
5		Frontal/Temporal	SAH (Fr; Temp); SDH (Fr)
6		Frontal	SDH
7		Frontal/Occipital	Contusion/SAH (Fr); SDH (Occ)
8		Frontal	SDH
9	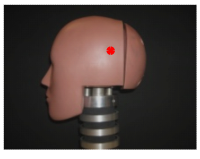	Parietal	SDH/SAH
10		Frontal/Parietal	Contusion (Fr); SAH (Par)

Table 3. Impact locations and lesion types of reconstructions 11-20. Fr = frontal; Temp = temporal; Par = Parietal; Occ = Occipital.

Case #	Impact location	Location of lesion	TBI Lesion
11		Parietal/Occipital	Contusion (Par); SDH (Occ)
12		Parietal/Occipital	EDH
13	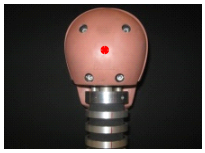	Occipital	SDH
14		Frontal/Occipital	Contusion (Fr); SDH (Occ)
15	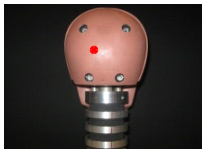	Frontal/Parietal	Contusion
16		Frontal	SDH
17		Frontal	SDH
18	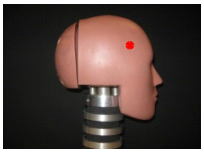	Parietal	SDH
19		Parietal	SDH
20		Parietal	SDH

Table 4. Table showing the total variance explained and the results of the rotated component matrix for contusions

omponent 1	Rotated Matrix Output	Component 2	Rotated Matrix Output	Component 3	Rotated Matrix Output	Component 4	Rotated Matrix Output
. lin time	0.956	X lin peak	0.924	Y lin peak	0.988	Z lin peak	0.937
. ang time	0.899	X lin slope	0.934	Y lin slope	0.979	Z lin slope	0.859
. lin time	0.950	X lin integral	0.888	Y lin integral	0.985	Z lin integral	0.887
. ang time	0.943	Y ang peak	0.934				
' lin time	0.951	Y ang slope	0.932				
' ang time	0.891	Y ang integral	0.925				
uration	0.954						
'ariance ccounted or	37.00%		23.80%		21.10%		11.10%
umulative	37.00%		60.80%		81.90%		93.00%

R = Resultant; lin = linear; ang = angular; time = time to peak; peak = peak magnitude

Table 5. Table showing the total variance explained and the results of the rotated component matrix for subdural hematoma

omponent 1	Rotated Matrix output	Component 2	Rotated Matrix output	Component 3	Rotated Matrix output	Component 4	Rotated Matrix output
lin time	0.982	X ang peak	0.953	X lin peak	0.94	Z ang peak	0.937
ang time	0.984	X ang slope	0.906	X lin slope	0.898	Z ang slope	0.938
lin time	0.982	X ang intergral	0.962	X lin integral	0.938	Z ang integral	0.872
ang time	0.964			Y ang peak	0.904		
lin time	0.971			Y ang integral	0.96		
ang time	0.979						
lin time	0.979						
uration	0.951						
ariance ccounted or	36.3%		18.7%		18.2%		12.0%
umulative	36.3%		54.9%		73.2%		85.1%

R = Resultant; lin = linear; ang = angular; time = time to peak; peak = peak magnitude

Table 6. Table showing the total variance explained and the results of the rotated component matrix for subarachnoid hemmorhage

'omponent 1	Rotated Matrix Output	Component 2	Rotated Matrix Output	Component 3	Rotated Matrix Output	Component 4	Rotated Matrix Output
. lin time	0.953	X lin peak	0.949	X ang peak	0.85	Z lin peak	0.9
. ang time	0.904	X lin slope	0.957	X ang slope	0.851	Z lin slope	0.902
: lin time	0.941	X lin integral	0.884	Z ang peak	0.898		
: ang time	0.922	Y ang peak	0.953	Z ang slope	0.898		
' lin time	0.957	Y ang slope	0.959	Z and integral	0.885		
' ang time	0.875	Y ang int	0.922				
)uration	0.942						
'ariance ccounted or	36.30%		23.90%		21.80%		11.10%
'umulative	36.30%		60.20%		81.90%		93.10%

R = Resultant; lin = linear; ang = angular; time = time to peak; peak = peak magnitude

Table 7. Table showing the total variance explained and the results of the rotated component matrix for epidural hematoma

Component 1	Rotated Matrix Output	Component 2	Rotated Matrix Output
R lin time	0.893	X lin peak	0.971
R ang time	0.877	X lin slope	0.973
X lin time	0.886	X lin integral	0.974
X ang time	0.868	Y lin peak	0.939
Y lin time	0.904	Y lin slope	0.952
Y ang peak	0.937	Y lin integral	0.926
Y ang time	0.864	Z ang integral	0.992
Z ang time	0.862		
Z ang slope	0.864		
Duration	0.919		
Variance accounted for	57.40%		37.20%
Cumulative	57.40%		94.60%

*R = Resultant; lin = linear; ang = angular; time = time to peak; peak = peak magnitude